

National Alzheimer's Project Act (NAPA)

The information that follows was included as an attachment to an email submitted by the public.

For more information about NAPA, visit the NAPA website at:

<http://aspe.hhs.gov/national-alzheimers-project-act>

Delayed K⁺ clearance associated with aquaporin-4 mislocalization: Phenotypic defects in brains of α -syntrophin-null mice

Mahmood Amiry-Moghaddam*, Anne Williamson[†], Maria Palomba[‡], Tore Eid[†], Nihal C. de Lanerolle[†], Erlend A. Nagelhus[§], Marvin E. Adams[¶], Stanley C. Froehner[¶], Peter Agre^{||}, and Ole P. Ottersen^{*,**}

*Centre for Molecular Biology and Neuroscience, University of Oslo, 0317 Oslo, Norway; [†]Department of Physiology and Biophysics, University of Washington, Seattle, WA 98195; [‡]Department of Neurosurgery, Yale University School of Medicine, New Haven, CT 06520; [§]National Centre for Epilepsy, 1303 Sandvika, Norway; [¶]Second University of Naples, 80138 Naples, Italy; and ^{||}Departments of Biological Chemistry and Medicine, Johns Hopkins University School of Medicine, Baltimore, MD 21205

Contributed by Peter Agre, September 17, 2003

Recovery from neuronal activation requires rapid clearance of potassium ions (K⁺) and restoration of osmotic equilibrium. The predominant water channel protein in brain, aquaporin-4 (AQP4), is concentrated in the astrocyte end-feet membranes adjacent to blood vessels in neocortex and cerebellum by association with α -syntrophin protein. Although AQP4 has been implicated in the pathogenesis of brain edema, its functions in normal brain physiology are uncertain. In this study, we used immunogold electron microscopy to compare hippocampus of WT and α -syntrophin-null mice (α -Syn^{-/-}). We found that <10% of AQP4 immunogold labeling is retained in the perivascular astrocyte end-feet membranes of the α -Syn^{-/-} mice, whereas labeling of the inwardly rectifying K⁺ channel, Kir4.1, is largely unchanged. Activity-dependent changes in K⁺ clearance were studied in hippocampal slices to test whether AQP4 and K⁺ channels work in concert to achieve isosmotic clearance of K⁺ after neuronal activation. Microelectrode recordings of extracellular K⁺ ([K⁺]_o) from the target zones of Schaffer collaterals and perforant path were obtained after 5-, 10-, and 20-Hz orthodromic stimulations. K⁺ clearance was prolonged up to 2-fold in α -Syn^{-/-} mice compared with WT mice. Furthermore, the intensity of hyperthermia-induced epileptic seizures was increased in approximately half of the α -Syn^{-/-} mice. These studies lead us to propose that water flux through perivascular AQP4 is needed to sustain efficient removal of K⁺ after neuronal activation.

Ever since the seminal finding of Hodgkin and Huxley (1) that nerve impulses lead to an efflux of K⁺, a major challenge in neurobiology has been to delineate the mechanisms for clearance of excess K⁺ from active neuropil. Efficient clearance of K⁺ is required to avoid interference with neuronal signaling. Notably, the buildup of K⁺ causes membrane depolarization that can induce synchronous discharges of nerve cells typical of overt seizures. Significant advances in understanding K⁺ clearance were made in early studies of retinal Müller cells. These glial cells, which span the entire thickness of the neural retina, were found to accumulate K⁺ from active neuropil and to siphon the excess K⁺ through the end-feet abutting on the corpus vitreum (2–4). It was later shown that activation of neuropil leads to a decrease in the extracellular space, suggesting uptake of water (5).

On the basis of these two sets of observations we hypothesized (6) that K⁺ clearance is coupled to water flux. If this coupling is obligatory, deficiency of the major brain water transport protein, aquaporin-4 (AQP4), would interfere with K⁺ clearance. Two lines of evidence support this hypothesis. First, immunogold studies showed a strict colocalization of AQP4 and Kir4.1 in the end-feet of retinal Müller cells (7). Second, activation of layer IV of freshly prepared rat cortical slices by high-frequency stimulation of thalamic afferents led to a concomitant flux of water and K⁺ toward the superficial cortical layers (8, 9).

In addition to retina (7), AQP4 is also concentrated in the perivascular astrocyte end-feet membranes in brain (6, 10, 11). At this location, AQP4 forms microcrystalline assemblies, referred to as square arrays (12), and the size of the arrays is regulated by the two isoforms of AQP4 (13). We recently demonstrated that mice homozygous for disruption of the gene encoding α -syntrophin (α -Syn^{-/-}) lack AQP4 in perivascular astrocyte end-feet membranes of neocortex and the molecular layer of cerebellum (14). AQP4 at these locations has been shown to confer bidirectional water flow between brain and blood (15).

In this study, we analyzed K⁺ clearance from hippocampus slices and seizure susceptibility in α -Syn^{-/-} mice (14). Functionally analogous to the Müller end-feet in the retina, perivascular astrocyte end-feet are believed to constitute the exit route for K⁺ and water from active neuropil throughout the brain. This analogy is supported by the findings that perivascular end-feet in the brain express Kir4.1, as shown by preembedding (16) and quantitative postembedding immunocytochemistry (present report). Together, our studies indicate that AQP4 water flux is needed to sustain efficient K⁺ clearance and that impaired water transport correlates with an increased intensity of epileptic seizures.

Materials and Methods

Animals. Experimental protocols were approved by the Institutional Animal Care and Use Committee and conform to National Institutes of Health guidelines for the care and use of animals. Studies were conducted with male mice homozygous for targeted disruption of the gene encoding α -syntrophin (17). WT C57Bl/6 mice were used as controls. α -Syn^{-/-} mice were bred on a C57Bl/6 background to avoid effects of differing genetic strains.

Antibodies. Rabbit polyclonal antibodies were obtained to AQP4 (Alpha Diagnostics, San Antonio, TX) and α -syntrophin (14, 15, 17). The antibody to Kir4.1 used for quantitative analyses was kindly provided by Yoshihisa Kurachi (Osaka University) (16). A second antibody to Kir4.1 was obtained commercially (Alpha-Diagnostics).

Immunogold Cytochemistry. Mice were killed and perfusion-fixed through the heart with 4% formaldehyde in phosphate buffer containing 0.2% picric acid at pH 6.0, then pH 10.0 (10, 15). Brains were cut into 0.5- to 1.0-mm slices, cryoprotected, quick-

Abbreviations: AQP4, aquaporin-4; [K⁺]_o, extracellular K⁺ concentration.

**To whom correspondence should be addressed at: Centre for Molecular Biology and Neuroscience, University of Oslo, P.O. Box 1105 Blindern, N-0317 Oslo, Norway. E-mail: o.p.ottersen@basalmed.uio.no.

© 2003 by The National Academy of Sciences of the USA

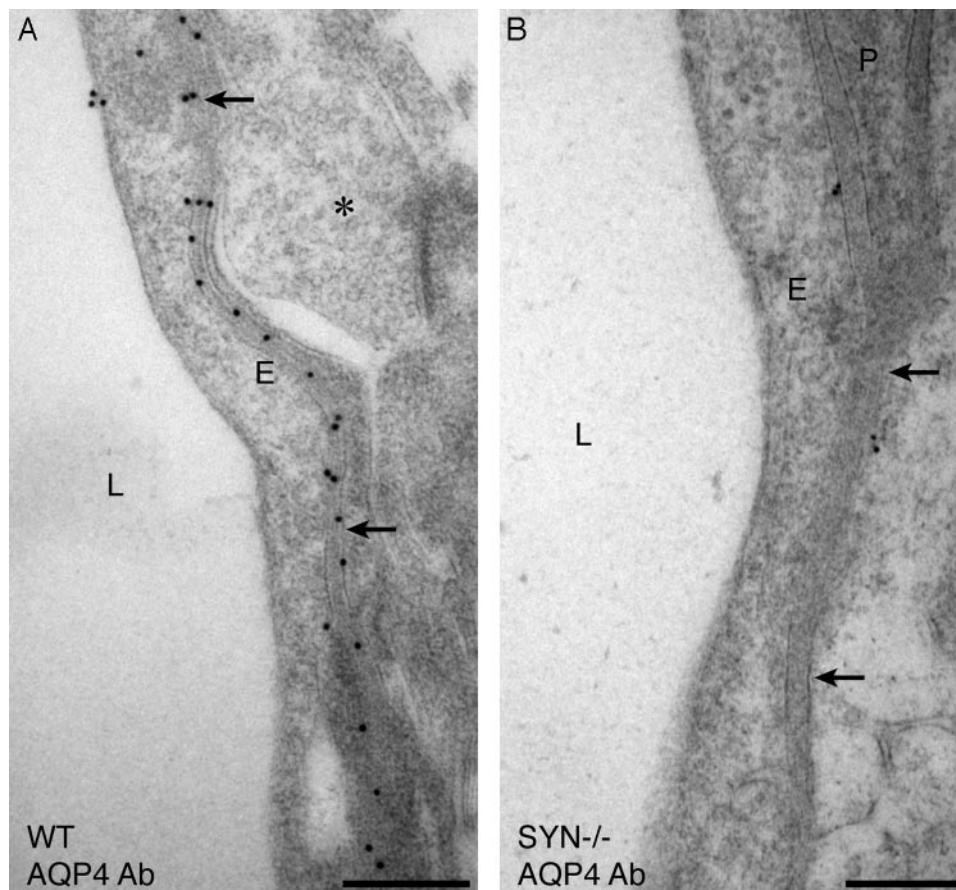


Fig. 1. Electron micrographs showing immunogold labeling of AQP4 in perivascular astrocyte end-feet of hippocampus. Corresponding ultrathin sections of brain from WT mouse (A) and α -Syn^{-/-} (B) mouse after immunogold labeling show markedly reduced labeling of AQP4 in the latter. L, lumen; E, endothelial cell; P, pericyte; arrows, perivascular membrane; *, unlabeled nerve terminal. (Bars = 0.5 μ m.)

frozen in liquid propane (-170°C), and subjected to freeze-substitution. Specimens were embedded in a methacrylate resin (Lowicryl HM20) and polymerized by UV light below 0°C . Ultrathin sections were incubated with antibodies to AQP4 (0.5 $\mu\text{g}/\text{ml}$), Kir4.1 (6 $\mu\text{g}/\text{ml}$ for the antibody provided by Y. Kurachi, or 0.003 $\mu\text{g}/\text{ml}$ for the Alpha Diagnostics antibody), or α -syntrophin (10 $\mu\text{g}/\text{ml}$) and visualized by staining with goat anti-rabbit IgG antibody coupled to colloidal gold and using a Philips CM 10 electron microscope at 60 kV.

Quantification and Statistical Analysis. For the quantification of AQP4 and Kir4.1 immunogold labeling, digital images of sections from three α -Syn^{-/-} mice and three WT mice (at least 10 images from each region for each animal) were acquired and quantified with a commercial image analysis program (Soft Imaging Systems, Münster, Germany) (15, 18). Comparisons between experimental groups were made by one-way ANOVA and post hoc Scheffé tests. Data are presented as mean \pm SEM.

Electrophysiology and Potassium Measurements. *In vitro* slice preparations were used (19). Briefly, 400- μm -thick slices were maintained in an interface recording chamber at 32.5°C . The tissue was kept oxygenated and perfused with artificial cerebrospinal fluid (ACSF) containing 124 mM NaCl, 3.5 mM KCl, 2 mM MgSO_4 , 1.2 mM NaH_2PO_4 , 26 mM NaHCO_3 , 2 mM CaCl_2 , and 10 mM dextrose, pH 7.4. For both CA1 layer and dentate gyrus recordings, the ion-selective recordings were made in the cell body layer and the stimulating electrodes were placed in the stratum radiatum (SR) or dentate molecular layer for ortho-

dromic activation. The electrode positions were adjusted to produce the maximal response in each slice. The minimal population spike amplitude was 5 mV in each area. No differences were noted in the peak population spike amplitude between the two groups of animals, indicating that slices from the Syn^{-/-} animals were not impaired during the slicing procedure.

We used double-barreled ion-selective electrodes to measure changes in extracellular K^+ concentration ($[\text{K}^+]_o$). The reference barrel (field potential electrode) was filled with 1 M NaCl, whereas the barrel used to measure $[\text{K}^+]_o$ was filled with the potassium ionophore 1 mixture B (Fluka). The tips of these double-barrel electrodes had a combined diameter of 8–10 μm and resistances of 1–10 m Ω for the reference electrode and 200–300 M Ω for the K^+ -selective electrode. Before and after each experiment, the ion-selective electrode was calibrated by using standard solutions, and experiments in which the variation exceeded 10% were rejected.

Hyperthermic Seizures. Mice were placed in a bath containing water at 45°C (20). At onset of seizure, the mice were removed and seizure intensity was graded on a modified version of Racine's six-point scale adopted for mice (21). In all cases, seizures appeared within 4 min of exposure to warm water.

Results

Immunogold Electron Microscopy of Hippocampus. The affinity-purified antibody specific for the C terminus of AQP4 was used to label ultrathin sections of hippocampus from WT mouse

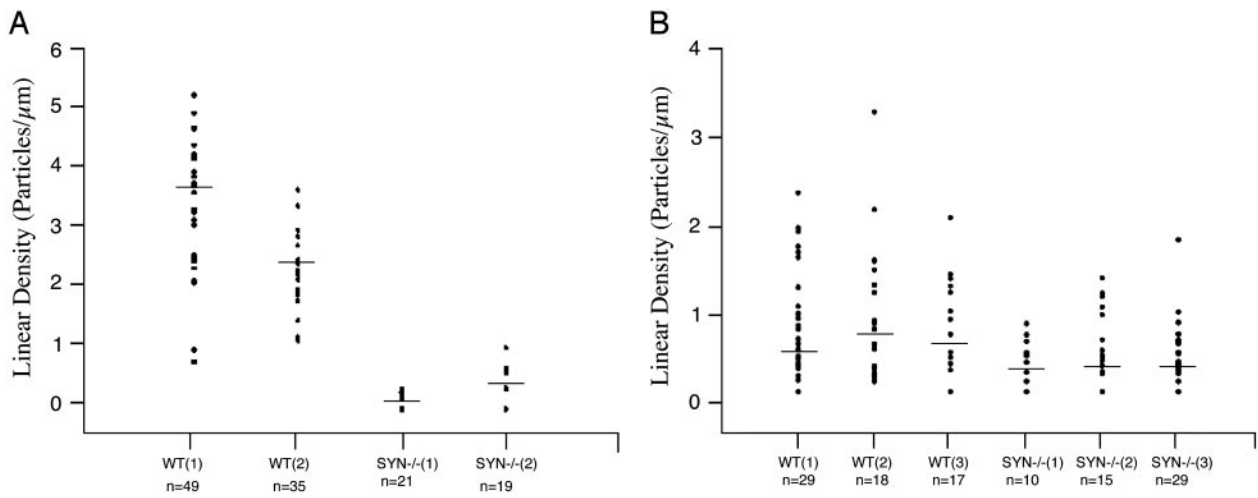


Fig. 2. Scatter plots showing the linear densities of immunogold labeling of AQP4 and Kir4.1 in perivascular astrocyte end-feet of hippocampus. (A) AQP4 labeling densities of preparations from two WT mice and two *Syn*^{-/-} mice are visibly different ($P < 0.001$ for each animal by post hoc Scheffé test). (B) Kir4.1 labeling densities of preparations from three WT and three *Syn*^{-/-} mice overlap with no statistically significant differences ($P = 0.4-0.8$). Each dot (y axis) represents the linear density of gold particles around a single capillary (n noted below x axis) in preparations from WT or *Syn*^{-/-} mice; horizontal bars represent median values.

brain. This produced a linear arrangement of immunogold particles beneath the basal laminae of capillary endothelia, a distribution corresponding to the perivascular membrane of

astrocytic end-feet (Fig. 1A). Evaluation of similar sections from *α-Syn*^{-/-} mice showed a striking mislocalization of AQP4 (Fig. 1B). The loss of AQP4 was equally pronounced in the stratum

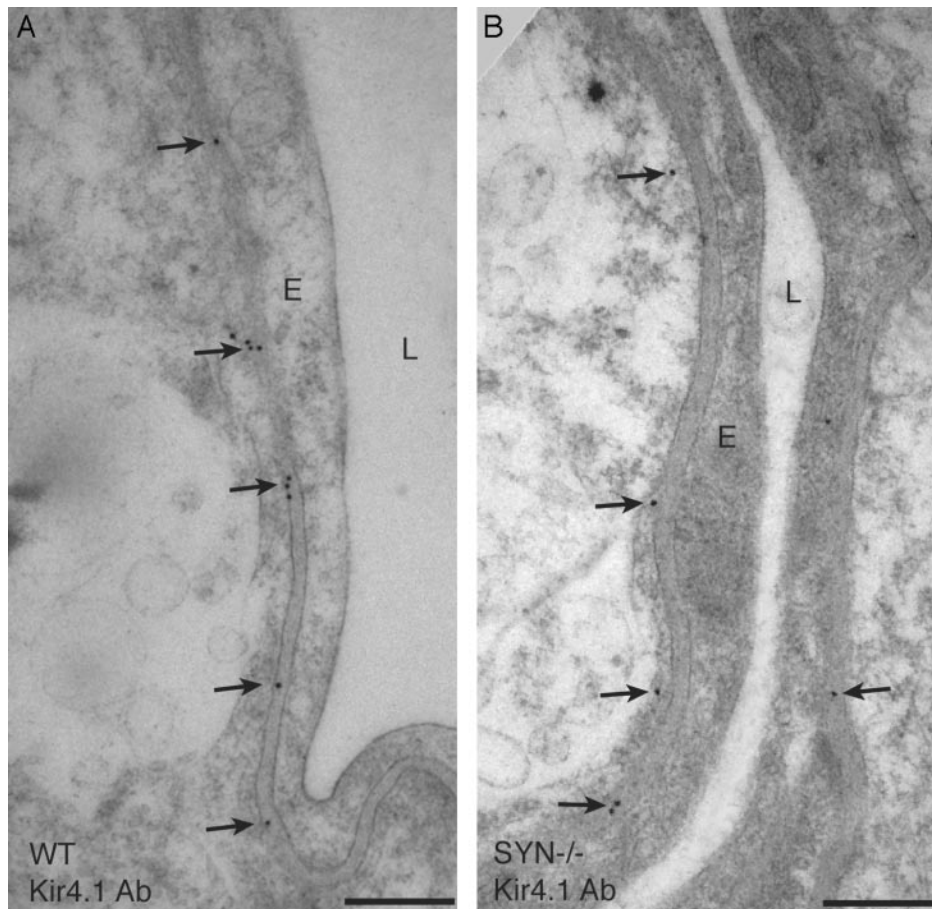


Fig. 3. Electron micrographs showing immunogold labeling of Kir4.1 in perivascular astrocyte end-feet of hippocampus. Corresponding ultrathin sections of brain from WT mouse (A) and *α-Syn*^{-/-} mouse (B) after immunogold labeling show a modest reduction of Kir4.1 labeling in the latter. L, lumen; E, endothelial cell; arrows, perivascular membrane. (Bars = 0.5 μm.)

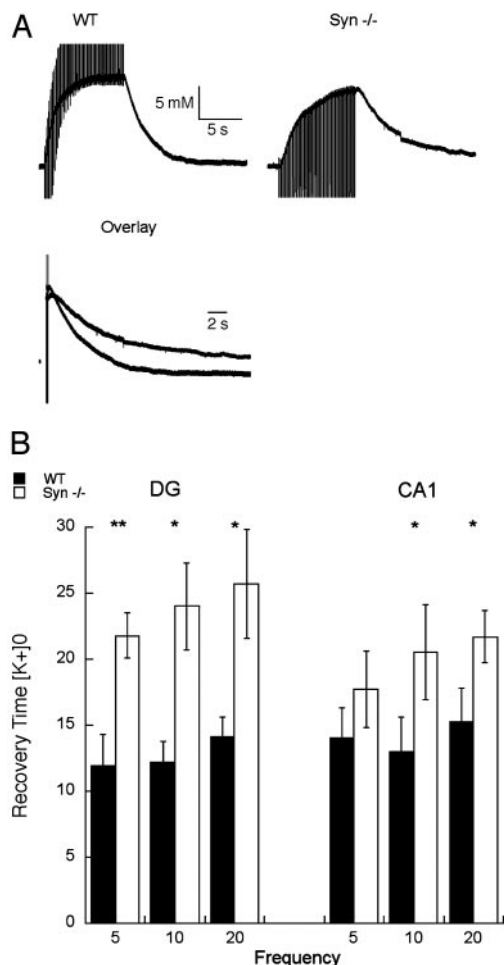


Fig. 4. Prolongation of the recovery of $[K^+]_o$ after repetitive orthodromic stimulation of isolated hippocampal slices. (A) Representative tracings of $[K^+]_o$ signal during and after a 10-Hz train delivered to the Schaffer collaterals from WT and α -Syn $^{-/-}$ mice shown separately or superimposed in overlay. (B) Pooled data from measurements taken from five WT mice and six α -Syn $^{-/-}$ mice. Plots represent time, in seconds, elapsed during recovery from 90% of peak value to the 10% level in CA1 and the dentate gyrus (DG). Data are shown as mean \pm SEM. *, $P < 0.05$; **, $P < 0.001$.

orients and the dentate molecular layer (not shown). Morphometric quantitation of immunogold labeling established that perivascular AQP4 labeling of α -Syn $^{-/-}$ samples was less than 10% of the level in hippocampus of WT mice (Fig. 2A). The loss of AQP4 immunogold labeling occurred only in perivascular membranes of astrocyte end-feet, because the immunogold signal for AQP4 was retained or even increased in other astrocyte membrane domains (not shown). As expected after disruption of the gene, anti- α -synaptrophin labeling was not detected in tissues from α -Syn $^{-/-}$ animals.

Earlier studies of retina revealed strict colocalization of AQP4 and the inwardly rectifying K^+ channel Kir4.1 in plasma membranes of Müller cell end-feet (7). Kir4.1 was similarly localized in perivascular membrane of astrocyte end-feet in the hippocampus of WT mice (Fig. 3A). However, when sections of hippocampus and retina were incubated simultaneously and under identical conditions, Kir4.1 immunogold labeling was found to be notably weaker in hippocampus with each of two different antibodies (not shown). Compared with that in WT mice, perivascular Kir4.1 immunogold labeling was only modestly reduced in hippocampus of α -Syn $^{-/-}$ mice (Fig. 3B). Morphometric comparisons of WT and α -Syn $^{-/-}$ hippocampus demon-

Table 1. Grading of hyperthermia-induced seizures in α -synaptrophin-null mice compared with WT mice

Score	WT	α -Syn $^{-/-}$	Description of the seizure (modified Racine scale)
6			Death
5		++	Clonus, rearing, falling, and rapid leg contractions
4		++	Clonus, rearing, and falling
3	+++	++	Clonus and rearing
2	++++++	+	Head nodding and forelimb clonus
1	+	++	Facial movement or silence
0			No response

Each + represents one mouse.

strated, on average, that at least 60% of the perivascular Kir4.1 labeling is retained in the mutant preparations (Fig. 2B), but the reduction was not consistent among animals, and the ranges of observations from WT and α -Syn $^{-/-}$ specimens overlapped (Fig. 2B). Thus, disruption of the α -synaptrophin gene causes a major rearrangement of AQP4 but only a modest perturbation of Kir4.1.

K^+ Flux After Neuronal Activation. Our initial hypothesis (6), that water flux through AQP4 plays a permissive role in synaptic K^+ homeostasis, predicts that α -Syn $^{-/-}$ mice will have delayed recoveries of $[K^+]_o$ after evoked activity. This prediction was tested in hippocampal slices *in vitro* by analyzing changes in $[K^+]_o$ induced by repetitive stimulation of afferent fiber pathways. Using ion-selective microelectrodes, we measured responses to 5-, 10-, and 20-Hz orthodromic stimulations to the Schaffer collaterals, for recordings in the CA1 layer, or to the perforant path, for recordings in the dentate gyrus. At least two series of recordings were made in each region for each animal, and a trend toward slightly higher peak $[K^+]_o$ values was observed with slices from WT animals (Fig. 4). The trend was not due to differences in amplitude of population spikes in either region when brain slices from WT and α -Syn $^{-/-}$ mice were directly compared: 7.9 ± 2.5 vs. 6.4 ± 1.9 mV (in CA1) and 12.8 ± 3.2 vs. 12.1 ± 2.8 mV (in dentate gyrus).

The $[K^+]_o$ recovery was measured by timing the number of seconds elapsed during the decline from 90% of the peak value to the 10% level. The recovery time was prolonged in hippocampal slices from α -Syn $^{-/-}$ mice when compared with corresponding slices from WT mice (Fig. 4A). The differences in $[K^+]_o$ recovery in both CA1 and the dentate gyrus were statistically significant in measurements after 10- and 20-Hz stimulation. These differences were more pronounced in the dentate gyrus than in CA1 at all frequencies (Fig. 4B). Regional differences may reflect the neuronal packing density and extracellular space volume, because smaller extracellular spaces will feature less dilution of K^+ released from active neurons (22).

Induction of Epileptic Seizures. Reduced efficiency of K^+ clearance after neuronal stimulation should be expected to increase the vulnerability to epileptic seizures. Hyperthermia is a simple experimental method to test for seizure susceptibility (20). The time elapsed from immersion in warm water to onset of the seizure was measured. Although not of statistical significance, seizures appeared sooner in α -Syn $^{-/-}$ mice (139 ± 12 s) than in WT mice (159 ± 10 s). The intensity of the seizures on the Racine scale was more severe in the α -Syn $^{-/-}$ mice, with four of nine animals reaching severity scores of 4 or 5 (clonus, rearing, falling, and sometimes repetitive leg contractions). In contrast, only three of ten WT mice reached a score of 3 (clonus and

rearing), and the other seven achieved scores of only 2 or below (head nodding, forelimb clonus, or facial movement or silence, Table 1).

Discussion

This study shows that disruption of the gene encoding α -syntrophin produces two major effects on brain function: perturbation of K^+ homeostasis by delaying the clearance after neuronal activation, and intensification of epileptic seizures induced by hyperthermia. The latter effect is most likely a consequence of the former, because increased $[K^+]_o$ is known to cause neuronal depolarization and epileptiform discharges.

The AQP4 water channel protein and α -syntrophin are strongly expressed in the perivascular membrane domains of astrocyte end-feet in the brains of WT animals. It has been established that these membrane domains show the most dramatic rearrangement of AQP4 distribution in neocortex and cerebellum of α -Syn^{-/-} mice (14, 15). Thus, the α -Syn^{-/-} mice have proven to be an invaluable tool for delineating the functions of this pool of AQP4 at the interface between blood and brain (15). Other parts of the astrocyte membrane retain their normal complement of AQP4 after α -syntrophin deletion, as do the kidney tubule cells. This retention implies that multiple mechanisms must exist to anchor AQP4 in the proper cellular location, and that only the perivascular pool of AQP4 in brain depends entirely on anchoring by α -syntrophin.

The α -Syn^{-/-} mouse model has previously provided evidence that the perivascular pool of AQP4 serves as an influx route of water in conditions associated with the development of brain edema (15). The aim of the present study was to use this model to explore the physiological function of AQP4. Specifically, we tested the hypothesis that water siphoning through perivascular AQP4 is essential for the handling of excess K^+ after neuronal activation. This hypothesis was prompted by our observation that Müller cells, the retinal equivalent of brain astrocytes, show strict subcellular colocalization of AQP4 with Kir4.1 (7), the K^+ channel believed to play a pivotal role in K^+ homeostasis. It has long been known that the retinal Müller cells take up K^+ from active neuropil and funnel excess K^+ into the corpus vitreum or blood vessels through their end-feet (4). Our observation that the Müller cell end-feet membranes are enriched in both AQP4 and Kir4.1 led us to suggest that activity-dependent K^+ fluxes are normally associated with water fluxes. Evidence in support of this view includes the observation that evoked activity in the deep layers of acute cortical slices induces concomitant water and K^+ fluxes directed toward the cortical surface (8, 9).

Here we show that genetic deletion of α -syntrophin slows the clearance of K^+ from active neuropil. This result emphasizes the importance of perivascular end-feet for normal brain function and provides support for the idea that the end-feet membranes are involved in K^+ homeostasis. As discussed above, the loss of perivascular AQP4 is the most impressive molecular defect found in α -Syn^{-/-} mice. Taken together, our data suggest that water transport not only is coupled spatially and temporally to K^+ clearance (9) but also is a prerequisite for efficient handling of excess K^+ .

The genetic deletion of α -syntrophin also caused a decrease in perivascular Kir4.1 that might have contributed to delayed K^+ clearance. Nevertheless, the reduction in Kir4.1 was modest compared with the reduction in AQP4 and was not consistent among animals. Like AQP4, Kir4.1 has a terminal SXV sequence that may attach to PDZ sequences in proteins of the dystrophin complex. Notably, mice lacking dystrophin (*mdx* mice) reveal a loss of Kir4.1 in Müller cell end-feet (23). The partial loss of Kir4.1 indicates that the protein interacts with other dystrophin-associated proteins. We also evaluated other molecules engaged in transport processes across the blood–brain interface, including monocarboxylate transporter 1 (MCT1), glucose transporter 1 (GLUT1), excitatory amino acid transporter 2 (EAAT2), and the NaKCl₂ cotransporter, but none were affected by genetic deletion of α -syntrophin as judged by postembedding immunogold analysis (data not shown).

In view of the observed delay in K^+ clearance, it was not surprising to find increased severity of induced seizures after genetic deletion of α -syntrophin. Finding only a minor change in seizure threshold, as measured by time required for onset of hyperthermia-induced seizures, can be interpreted because α -syntrophin does not affect the functional properties of non-end-foot membranes of astrocytes. These membranes remain available for K^+ and water uptake. One could envisage that the efflux route through glial end-feet may become critical only at high K^+ concentrations, known to occur after onset of seizures. This behavior might also explain why the α -Syn^{-/-} animals appeared to cope slightly better with the extracellular K^+ at low than at high stimulation intensities, consistent with the normal behavior of these mice under control conditions.

Why should K^+ clearance be contingent on water transport? In principle, spatial buffering of K^+ should be independent of water movement, because the net ion flux is very small (24). However, K^+ uptake occurs by several mechanisms, some of which have been shown to lead to cell swelling and water uptake in isolated cells (25–28). K^+ transport that generates an osmotic gradient will be facilitated if accompanied by water flux. We believe this mechanism underlies the observations reported here. In sum, our findings suggest that the functional integrity of perivascular end-feet is essential for efficient clearance of K^+ during high neuronal activity. Thus water and K^+ transport are handled by separate membrane proteins that are functionally coupled and interdependent and share the same polarized distribution. It follows that an impaired polarization of astrocytes, as seen in certain types of gliosis and other clinical disorders of the central nervous system, will be of pathophysiological importance in clinical epilepsy. This conclusion adds an important disease to the list of clinical disorders possibly involving aquaporins.

We thank Swerine Amarasingha for technical assistance and Annibale A. Puca and Donald L. Price for critical evaluations of the manuscript. This work was supported in part by grants from the National Institutes of Health, the Norwegian Research Council, and European Cooperation in Scientific and Technological Research (COST).

1. Hodgkin, A. L. & Huxley, A. F. (1952) *J. Physiol. (London)* **117**, 500–544; reprinted (1990) *Bull. Math. Biol.* **52**, 25–71.
2. Karwoski, C. J., Lu, H. K. & Newman, E. A. (1989) *Science* **244**, 578–580.
3. Paulson, O. B. & Newman, E. A. (1987) *Science* **237**, 896–898.
4. Newman, E. A., Frambach, D. A. & Odette, L. L. (1984) *Science* **225**, 1174–1175.
5. Holthoff, K. & Witte, O. W. (1996) *J. Neurosci.* **16**, 2740–2749.
6. Nielsen, S., Nagelhus, E. A., Amiry-Moghaddam, M., Bourque, C., Agre, P. & Ottersen, O. P. (1997) *J. Neurosci.* **17**, 171–180.
7. Nagelhus, E. A., Horio, Y., Inanobe, A., Fujita, A., Haug, F. M., Nielsen, S., Kurachi, Y. & Ottersen, O. P. (1999) *Glia* **26**, 47–54.
8. Holthoff, K. & Witte, O. W. (2000) *Glia* **29**, 288–292.
9. Niermann, H., Amiry-Moghaddam, M., Holthoff, K., Witte, O. W. & Ottersen, O. P. (2001) *J. Neurosci.* **21**, 3045–3051.
10. Nagelhus, E. A., Veruki, M. L., Torp, R., Haug, F. M., Laake, J. H., Nielsen, S., Agre, P. & Ottersen, O. P. (1998) *J. Neurosci.* **18**, 2506–2519.
11. Frigeri, A., Gropper, M. A., Umenishi, F., Kawashima, M., Brown, D. & Verkman, A. S. (1995) *J. Cell Sci.* **108**, 2993–3002.
12. Rash, J. E., Yasumura, T., Hudson, C. S., Agre, P. & Nielsen, S. (1998) *Proc. Natl. Acad. Sci. USA* **95**, 11981–11986.
13. Furman, C. S., Gorelick-Feldman, D. A., Davidson, K. G. V., Yasumura, T., Neely, J. D., Agre, P. & Rash, J. E. (2003) *Proc. Natl. Acad. Sci. USA* **100**, 13609–13614.
14. Neely, J. D., Amiry-Moghaddam, M., Ottersen, O. P., Froehner, S. C., Agre, P. & Adams, M. E. (2001) *Proc. Natl. Acad. Sci. USA* **98**, 14108–14113.

